Mineralogical Magazine, November 2015, Vol. 79(6), pp. 1353–1367

OPEN ACCESS

Characterizing mineralogy and redox reactivity in potential host rocks for a UK geological disposal facility

J. Quirke[1], C. M. B. Henderson[2,6], R. A. D. Pattrick[2], K. M. Rosso[2,3], A. Dent[4], J. W. Sharples[5] and C. I. Pearce[1,*]

[1] School of Chemistry and Dalton Nuclear Institute, University of Manchester, Oxford Road, Manchester M13 9PL, UK
[2] School of Earth, Atmospheric and Environmental Sciences, University of Manchester, Oxford Road, Manchester M13 9PL, UK
[3] Pacific Northwest National Laboratory, Richland, Washington, 99352, USA
[4] Diamond Light Source, Didcot, Oxfordshire OX11 0DE, UK
[5] Photon Science Institute, University of Manchester, Oxford Road, Manchester M13 9PL, UK
[6] ASTeC, STFC Daresbury Laboratory, Warrington WA4 4AD, UK

[*Received 28 October 2014; Accepted 09 July 2015; Associate Editor: Nick D. Bryan*]

ABSTRACT

Geological disposal facilities (GDF) are intended to isolate and contain radioactive waste within multiple protective barriers, deep underground, to ensure that no harmful quantities of radioactivity reach the surface environment. The last line of defense in a multi-barrier GDF is the geosphere, where iron is present in the host rock mineralogy as either Fe(II) or Fe(III), and in groundwater as Fe(II) under reducing conditions. The mobility of risk-driving radionuclides, including uranium and technetium, in the environment is affected significantly by their valence state. Due to its low redox potential, Fe(II) can mediate reduction of these radionuclides from their oxidized, highly mobile, soluble state to their reduced, insoluble state, preventing them from reaching the biosphere. Here a study of five types of potential host rocks, two granitoids, an andesite, a mudstone and a clay-rich carbonate, is reported. The bulk rocks and their minerals were analysed for iron content, Fe(II/III) ratio, and for the speciation and fine-grained nature of alteration product minerals that might have important controls on groundwater interaction. Total iron content varies between 0.9% in clays to 5.6% in the andesite. X-ray absorption spectroscopy reveals that Fe in the granitoids and andesite is predominantly Fe(II), and in mudstones, argillaceous limestone and terrestrial sandstone is predominantly Fe(III). The redox reactivity of the potential host rocks both in the presence and absence of Fe(II)-containing 'model' groundwater was investigated using an azo dye as a probe molecule. Reduction rates as determined by reactivity with the azo dye were correlated with the ability of the rocks to uptake Fe(II) from groundwater rather than with initial Fe(II) content. Potential GDF host rocks must be characterized in terms of mineralogy, texture, grain size and bulk geochemistry to assess how they might interact with groundwater. This study highlights the importance of redox reactivity, not just total iron and Fe(II)/(III) ratio, when considering the host rock performance as a barrier material to limit transport of radionuclides from the GDF.

* E-mail: Carolyn.Pearce@manchester.ac.uk
DOI: 10.1180/minmag.2015.079.6.11

The publication of this research has been funded by the European Union's European Atomic Energy Community's (Euratom) Seventh Framework programme FP7 (2007–2013) under grant agreements n°249396, SecIGD, and n°323260, SecIGD2.

Keywords: geosphere, iron-bearing minerals, Fe(II)/Fe(III) ratio, reducing potential, X-ray absorption spectroscopy, granitoids, andesite, mudstone, clay-rich carbonate.

Introduction

The UK government has set out a framework for the long-term management of high activity radioactive waste in a geological disposal facility (GDF) in the recent white paper by the Department of Energy & Climate Change (2014). All the proposed GDF's incorporate a multi-barrier system to isolate the waste from the surrounding environment and to contain the decaying radioactivity for >100,000 years (Nuclear Decommissioning Authority, 2010). The multi-barrier concept involves a waste package, consisting of the waste form, e.g. high-level radioactive waste in glass, and the waste container e.g. a stainless steel container. This waste package is enclosed in an engineered barrier, e.g. clay, to minimize water flow around the waste container for several hundred years. Over longer times, when these engineered barriers are no longer intact due to inevitable chemical and physical degradation, the 'safety function' of the host rock is to contain the radionuclides released from the waste package, limiting their migration into the biosphere. As a site has not yet been selected for a UK GDF, the screening of potential candidate host lithologies is essential to support the implementation of geological disposal by Radioactive Waste Management (RWM) Ltd. Important geospheric aspects for the GDF site selection process include choosing the type of rock, defining the mineralogy and its reactivity, especially the presence of redox active phases, and the nature of fine-grained alteration products (very large surface areas). Redox active elements, such as iron, present within the rock, can influence the oxidation state of long-lived radioactive elements including uranium, plutonium, technetium and neptunium, which determines their solubility and, consequently, their mobility in the environment.

Here, we characterize the iron content, its chemical form and the Fe(II/III) ratio in six samples, including five potential host rocks of contrasting mineralogy (granitoids, volcanic, mudstone and carbonate), along with a ferruginous sandstone from one the of the UK's major aquifers; the aim is to determine how Fe(II/III) ratio influences redox reactivity. Granitic and volcanic lithologies are representative of higher strength crystalline rocks and fine-grained clastics are lower strength sedimentary rocks, as defined by the Nuclear Decommissioning Agency (2010). Four of the six samples are from western Cumbria, which was subject to a (failed) application for a GDF rock facility in 1997 and which volunteered for exploration for potential GDF sites in 2012–2013. The Ordovician Borrowdale Volcanic Group (BVG) forms the central component of the Lake District massif, and comprises subduction-related, K-rich, calc-alkaline andesites (Millward, 2004). It formed ~456 ± 2 Ma and was subsequently subjected to late Caledonian (Acadian, 395 Ma) regional, sub-greenschist facies metamorphism. It has also been subjected to nine stages of hydrothermal activity leading to complex veining and associated wall-rock alteration (Milodowski *et al.*, 1998). The sample examined here (BV3) is from the Birker Hill Andesite Formation (Millward, 2004).

The 450 ± 3 Ma Eskdale Granite is a component of the Lake District Batholith at the western margin of the Lake District massif. The northern part is a coarse-grained granite, and the southern is granodioritic; chloritic alteration is widespread in places and intense when related to granophile hydrothermal mineralization (Young *et al.*, 1986; Millward, 2004). The samples studied are one relatively unaltered sample (15228) from the granitic intrusion at Linbeck Quarry, and the second (15224) is from the more altered granodiorite from Wabberthwaite Quarries.

Two Jurassic lithologies were examined. One sample from the Lower Lias is a mudstone from the Blue Clay east of Lyme Regis where these formations have been buried >2 km (Kiriakoulakis *et al.*, 2000; Hesselbo, 2008). The second sample is an argillaceous limestone from the Oxford Clay, at Quest Pit, Stewartby, Bedfordshire (MacQuaker, 1994; Barron *et al.*, 2012).

The St Bees sandstone (Sherwood Sandstone Group) is a largely fluviatile sandstone sequence deposited in the semi-arid conditions of the Triassic (~240 Ma) The red (authigenic hematite) sandstone was only buried shallowly (Burley, 1984) and the sample comes from the Sheetflood sandstones at St Bees Head (Holliday *et al.*, 2005).

The rocks were characterized using X-Ray Fluorescence (XRF), X-Ray Diffraction (XRD), Electron Probe Micro-Analysis (EPMA), Electron Paramagnetic Resonance (EPR), and X-Ray Absorption Spectroscopy (XAS). Redox reactivity was investigated by simulating the reducing conditions expected to be present in the groundwater-saturated host rock through the addition of Fe(II); then monitoring the reduction of the azo-

chromophore in Remazol Black B to the corresponding colourless amines.

Experimental Methods

Characterization of rocks

XRF

Major-element analyses were obtained with a wavelength dispersive, PANanalytical Axios spectrometer using the standard glass AUSMON (B255). Finely powdered rock sample (12 g) and fine powdered wax (3 g) were milled for 7 min at 350 rpm in a TEMA mill and pressed into a pellet at 10 tonnes.

$H_2O(-)$ and loss on ignition

Samples (1 g) were dried at 100°C for 1 hr, cooled in a desiccator and weight loss recorded to determine the loosely held water, $H_2O(-)$. Samples were then heated for 1 hr at 1100°C, cooled in a desiccator and reweighed. The loss on ignition is due to dehydroxylation of hydrous phases (e.g. micas, chlorite, clay minerals) and to release of CO_2 by breakdown of carbonates and oxidation of organic matter.

XRD

Samples (0.95 g) were ground with a silicon standard (0.05 g), packed into well-mounts and run on a Philips X'Pert diffractometer using Cu$K\alpha$ radiation. A step size of 0.0033°2θ with a counting time of 0.5 s per step over a 2θ range of 5–90° was used. Powder patterns were fitted using a search/match routine (*EVA* software programme).

EPMA

Samples were prepared as polished ~30 μm thin sections and carbon coated. Analyses was undertaken using a Cameca SX100 electron microprobe operated at 20 keV, beam current 20 nA, and spot size 2 μm. Mineral and oxide samples were used as standards. Analyses were recalculated to a standard number of oxygens per formula unit (p.f.u.). Hydrous minerals were calculated on an (OH)-free basis: micas to 22(O); chlorite to 28(O); epidote to 12.5(O). For some minerals of known stoichiometry, model Fe^{2+} – Fe^{3+} ratios were calculated assuming strict stoichiometry where possible (Droop, 1987).

EPR

The EPR spectra were obtained at 295 K using an EMX Micro X-band spectrometer with a microwave frequency of 9.5 GHz and a 1.0 T electromagnet. Samples were prepared by mounting 0.3 g powder in a fused quartz tube.

XAS

Powdered samples were diluted with cellulose to give the necessary absorption coefficient for the Fe *K*-edge (edge step 1–2) and pressed into pellets (13 mm). These were sealed in Kapton tape in a sample holder. Fe *K*-edge X-ray absorption spectra were obtained at the Diamond Light Source beamline B18 (SP4941). Samples were measured in fluorescence mode with Fe foil as an energy calibration standard after the third ion chamber. The beam current was 135 mA and spectra were scanned from 6950 to 7962 eV in triplicate by 5 min fast EXAFS scans (QUEXAFS) with a step size of 0.35 eV.

Redox reactivity of rock samples

Reducing potential under anaerobic conditions

Experiments were carried out to determine if the different rock types could reduce the reactive azo dye, Remazol Blue Black (RBB), under anaerobic conditions (Pearce *et al.*, 2006). RBB dye (6 ml, 0.1 mM) was added, using a syringe with a 0.22 μm filter, to sealed anaerobic serum bottles containing HEPES (4-(2-hydroxyethyl)-1-piperazineethanesulfonic acid) buffer (14 ml, 1 mM) and 0.2 g (containing ~0.1 mM total Fe) of powdered rock sample (TEMA mill, 2 mins) that had been sterilized (1 hr at 80°C) to remove any effect of microbial activity, giving a final dye concentration of 0.03 mM. The bottles were sampled at regular intervals over 60 days and centrifuged (4000 rpm, 5 min) prior to measurement of absorbance at the λ_{max} for RBB (597 nm) using a Shimadzu UV-1800 UV-vis spectrophotometer.

Iron sorption and effect on reducing potential

Experiments were carried out to determine how much Fe(II) the different rock types could adsorb from reducing groundwater, thereby increasing the reduction potential. Under anaerobic conditions, samples (0.2 g) were exposed to solutions containing $Fe(II)Cl_2.4H_2O$ (0.1 mM) and the concentration of Fe(II) removed from solution was measured using the ferrozine assay (Stookey, 1970). After 10 days, the Fe(II) solution was extracted, the HEPES buffer was added and the samples were sterilized as described previously. The RBB dye was added and the absorbance measured at 597 nm to determine if the different rock types could reduce the dye after exposure to Fe(II)-containing solution.

Controls containing the Fe(II) solution and RBB dye were prepared to determine the effect of Fe(II) on the dye in the absence of the rock samples.

Results and discussion

Petrography and analyses of minerals and bulk rock samples

Minerals were characterized using electron microprobe X-ray scans, EPMA spot analyses, and powder XRD traces. X-ray maps are particularly useful for characterizing the nature of groundmass minerals and fine-grained alteration products as these phases are likely to be the most reactive to migrating fluids because of their large surface areas.

Eskdale Granitic intrusions (15228 and 15224)
Sample 15228 is a typical coarse-grained granite. Plagioclase phenocrysts tend to have relatively unaltered Na-rich rims with pervasively altered cores with remnant patches of more calcic feldspar (Table 1, analysis 4). Alkali feldspars are generally less altered than the plagioclases and this is the usual relationship for granitoids from the Eskdale intrusion (Simpson, 1934). Note that the intense alteration of both plagioclase and alkali feldspar is reflected in the stoichiometry departing from ideal Si:Al feldspar ratios. The common excess of Al over Si is likely to indicate the presence of fine-grained aluminous clay minerals as major alteration products. X-ray maps of pervasively altered primary feldspars show compositional heterogeneities on a length-scale of ~3–10 μm which matches the sizes of clay minerals and interlayered grains of mica – chlorite – clay formed by low-temperature alteration of igneous rocks (Peters and Hofmann, 1984; Psyrillos *et al.*, 1999).

Biotite is abundant, forming lath-shaped (up to 1 mm) and more irregular grains with incipient alteration along cleavages to chlorite. Chlorite is also present as larger grains; average biotite and chlorite analyses are given in Table 1 (analyses 1 and 2, respectively). Note that the relatively low K content in the biotite probably reflects the first stages of K loss during alteration to chlorite. It is not possible to calculate model $Fe^{2+} - Fe^{3+}$ contents for either biotite or chlorite because of partially filled structural units but both minerals are likely to have Fe^{2+} as the main valency state (Deer *et al.*, 1962; Fleet, 2003). The primary biotite and its chloritic alteration product have similar Fe/Mg

TABLE 1. Representative results of analyses of the minerals by EPMA.

	Granite 15228					Granite 15224			Andesite BV3		Mudstone OM			Sandstone SBS
	Biotite	Chlorite	Epidote	Plag. core	Plag. rim	Phengite	Chlorite	Magnetite	Chlorite	Perthite	Chlorite	Na-feld	K-feld	Magnetite
Analysis	1	2	3	4	5	6	7	8	9	10	11	12	13	14
Wt.%	Av. of 8		Av. of 2			Av. of 7	Av. of 4	Av. of 10	Av. of 3					
SiO_2	34.13	28.73	39.04	54.07	65.61	50.82	27.56	0.11	25.69	67.21	25.53	68.64	64.52	0.49
TiO_2	2.79	1.10	0.06			0.19	0.06	0.84	0.03		0.07			0.14
Al_2O_3	16.51	17.67	28.98	28.03	23.49	30.12	19.45	0.03	20.06	20.61	22.27	20.86	19.36	0.24
FeO	25.81	30.26	5.84	0.02*	0.12*	4.39	20.52	86.80	29.24	0.19*	28.91	0.19*	0.19*	84.40
MnO	0.58	0.72	0.16			0.01	0.18	0.03	1.43		0.70			0.07
MgO	5.59	6.76	0.02			2.98	18.82	0.01	9.83		9.14			0.05
CaO	0.03	0.07	23.96	12.34	2.79	0.04	0.08		-	0.17	0.23	0.51	0.77	
Na_2O	0.07	0.02	-	4.90	8.29	0.07	-		-	6.66	0.05	10.70	0.38	
K_2O	8.51	3.01	-	0.20	0.20	8.95	-		0.28	5.73	0.07	0.07	13.96	
Total	94.03	88.35	98.04	99.64	100.51	97.56	86.67	87.82	86.55	100.55	86.97	100.85	99.16	85.39

Cations														
No. of O (p.f.u.)	22(O)	28(O)	12.5(O) and 3Si	8(O)	8(O)	22(O)	28(O)	32(O) and 24 cations	28(O)	8(O)	28(O)	8(O)	8(O)	32(O) and 24 cations
Si	5.457	6.271	3.000	2.460	2.852	6.611	5.714	0.036	5.647	2.965	5.530	2.963	2.974	0.164
Al	2.543	1.729		1.503	1.204	1.389	2.286		2.353	1.072	2.470	1.061	1.052	
Sum Z	8.000	8.000				8.000	8.000		8.000		8.000			
Al	0.569	2.818	2.625			3.230	2.467	0.011	2.844		3.215			0.094
Ti	0.336	0.180	0.003			0.019	0.009	0.206	0.005		0.011			0.035
Fe	3.451	5.525	Fe^{3+} 0.356 Fe^{2+} 0.019	0.001*	0.004*	0.478	3.558	Fe^{3+} 15.504 Fe^{2+} 8.229	5.375	0.006*	5.237	0.006*	0.007*	Fe^{3+} 15.506 Fe^{2+} 8.156
Mn	0.078	0.132	0.011			0.001	0.032	0.008	0.266		0.128			0.018
Mg	1.333	2.200	0.002			0.578	5.817	0.005	3.220		2.950			0.025
Sum Y	5.767					4.306								
Ca	0.005	-	1.973	0.602	0.130	0.005	0.018		0.018	0.008	0.054	0.024	0.038	
Na	0.03	-	-	0.432	0.698	0.016				0.570	0.022	0.896	0.034	
K	1.735	0.838	-	0.012	0.011	1.485			0.077	5.73	0.018	0.004	0.821	
Sum X		11.693					11.901		11.787		11.635			
Total	15.530	19.693	7.989			13.812	19.901		19.787		19.635			
Mole %														
An				59.0	16.2					0.9		2.7	4.3	
Ab				39.9	82.4					61.9		96.8	3.6	
Or				1.1	1.4					37.2		0.5	92.1	

* Fe as Fe(III)

ratios (Table 1). Opaque Fe-oxides form grains up to 0.15 mm and occur as inclusions in the main silicates as well as groundmass phases; EPMA analyses show that the main oxide is an ilmenite with 6.9 wt.% MnO. Epidote is present in small amounts reflecting late-stage alteration; this phase has very low Mg and is rich in Fe^{3+} (Table 1, analysis 3). The EPMA analyses of calcite show the presence of 0.2 wt.% MgO, 0.3 wt.% FeO and 1.3 wt.% MnO.

The granodioritic component of the Eskdale granite intrusion is represented by sample 15224. Plagioclase and alkali feldspars are more altered than those in sample 15228. Both feldspar species are riddled with small lath-shaped grains of muscovite and are stained brown by clay-mineral alteration. Prismatic sub-grains (~2 × 1 mm) consisting of laminated intergrowths of small flakes of white mica also contain chlorite and are likely to be pseudomorphs after biotite or hornblende. Chlorite also forms patches up to 3 mm across often associated with small grains of Fe oxide (<0.2 mm). Carbonate is present in patchy (2 mm) alteration zones.

An optical image (plane polarised light) of a 'white' mica intergrowth with chlorite alteration zones is shown in Fig. 1*a*; the textural relations are clear in the Mg, and Al X-ray maps (Figs 1*c* and *b*, respectively). The flakes in the mica region are typically 50–100 μm × 5–10 μm in size. The distribution of red/yellow (false-colour images) grains in the Fe and Mg maps (Figs 1*d* and *c*) mark the chlorite regions clearly. The larger, red grains in the Ca map are apatite. The EPMA analysis of the

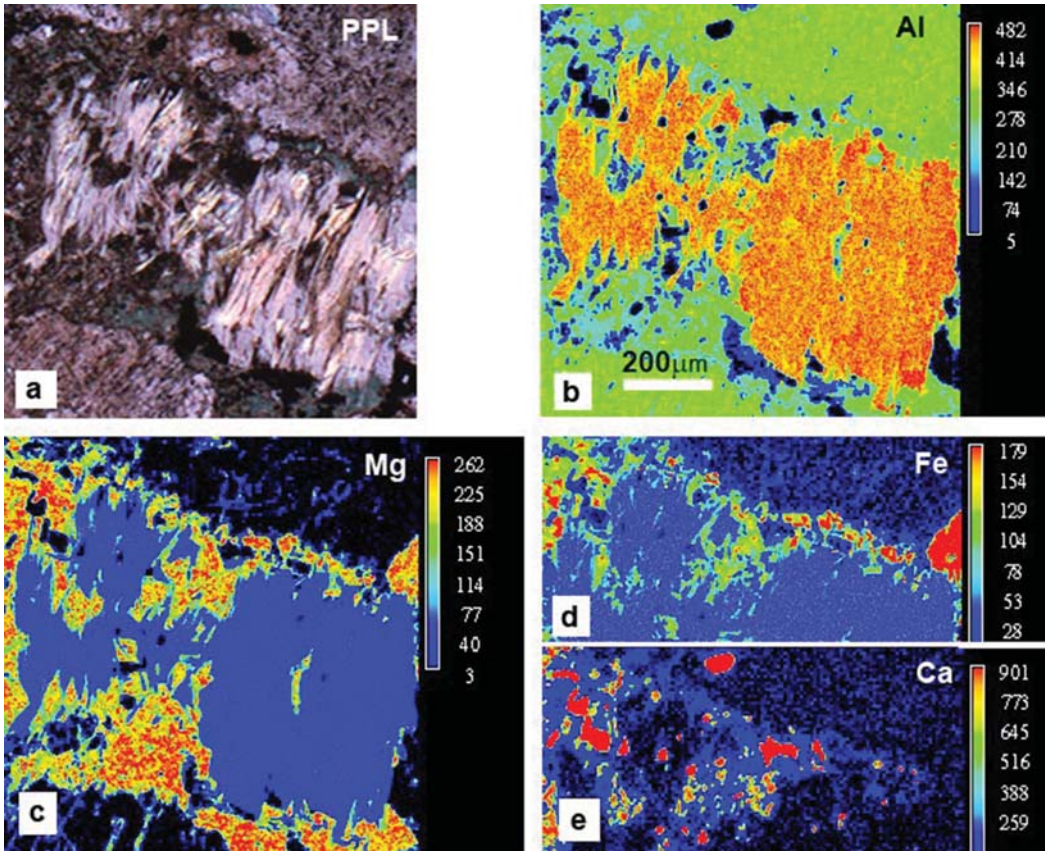

FIG. 1. Photomicrographs and X-ray maps for Eskdale granite 15224; all images are on the same scale: (*a*) Plane polarised light (ppl) image of phengite-chlorite pseudomorph after bitotite. (*b–f*) False colour X-ray maps: (*b*) Al – note that the scale bar is 200 μm; (*c*) Mg; (*d*) Fe; (*e*) Ca. Note that panels (*d*) and (*e*) match the top halves of the other panels. See text for further details.

mica in sample 15224 shows that it is characterized by being Si-rich and Al-poor with significant Fe, Mg and Ti contents and can be classified as phengite (Table 1, analysis 6). It is not possible to model its Fe valency ratio because of partially filled octahedral and interlayer structural units but Fe^{2+} is

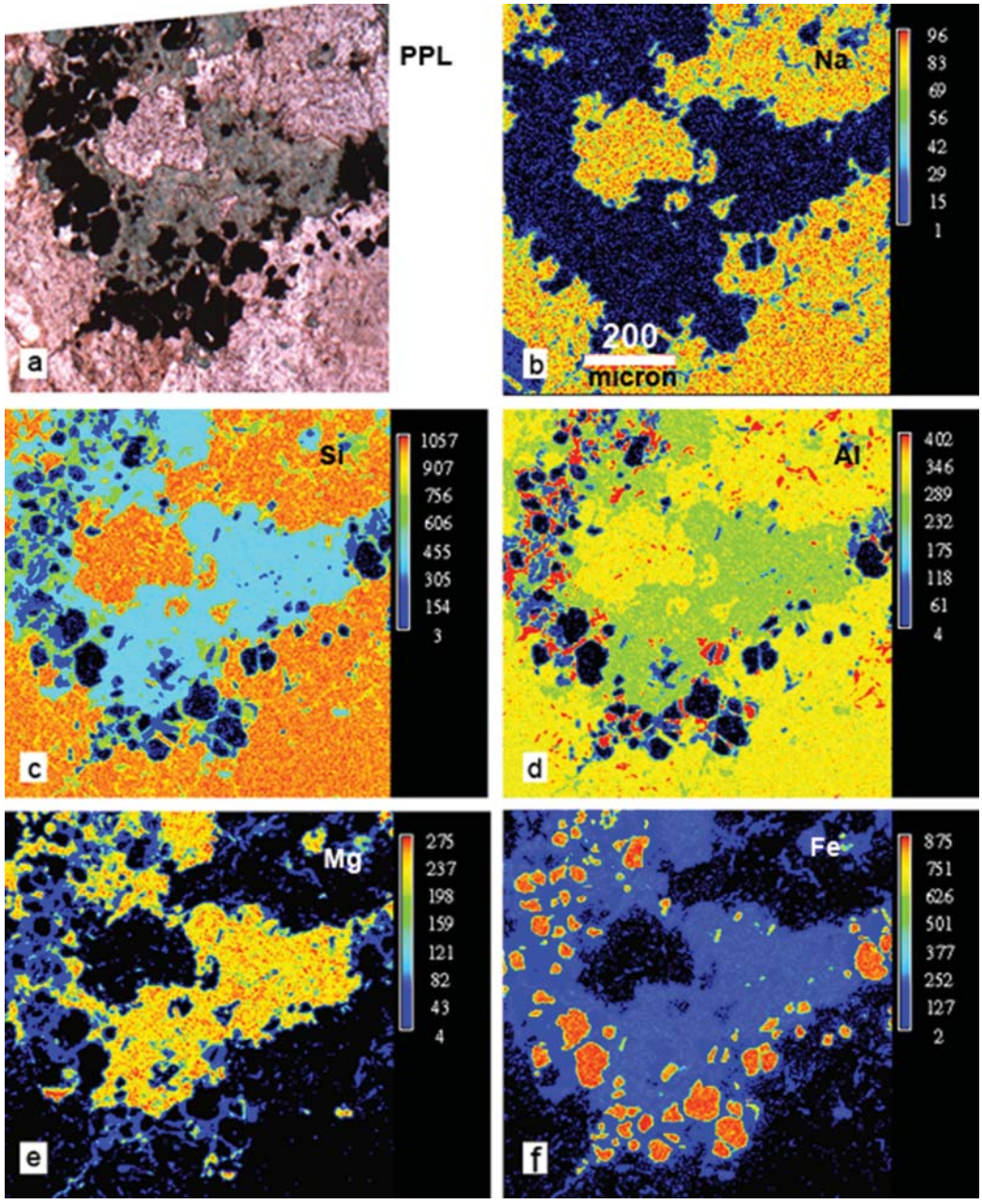

FIG. 2. Photomicrographs and X-ray maps for Eskdale granite 15224; all images are on the same scale: (*a*) Plane polarised light (ppl) image of a region with chlorite grains and associated magnetites. (*b–f*) False colour X-ray maps: (*b*) Na – note that the scale bar is 200 μm; (*c*) Si; (*d*) Al; (*e*) Mg; (*f*) Fe. See text for further details.

probably present in significant amounts because the phengite substitution mechanism is conventionally defined as $(Fe^{2+},Mg)_{oct} + Si_{tet}$ substituting for $(Al, Fe^{3+})_{oct} + Al_{tet}$ (Fleet, 2003).

Figure 2*a* shows another region in sample 15224 with an intimate intergrowth of Fe-oxides and chlorite with adjacent grains of severely altered feldspars. The Fe map (Fig. 2*f*) shows small sub-rounded Fe oxides (~5–10 μm) and the X-ray maps for Mg (yellow/red regions) (Fig. 2*e*) and Al (pale green) (Fig. 2*d*) display a large poikilitic grain of chlorite. The Na (Fig. 2*b*) and Al maps show the presence of several grains of Na-rich alkali feldspar. Similar sized separate grains of K-feldspar also occur in this rock and both of these feldspars show pervasive alteration to fine grained (5–10 μm), clay minerals.

The EPMA analyses show that the Fe-oxides are low-Ti magnetites (Table 1, analysis 8). Although modelling the Fe valency content using Droop's formula (recalculation to 4 O and 3 cations) provides cell formulae close to ideal magnetite it is probable that it is an oxidized maghemite-rich spinel with <3 cations p.f.u. due to the presence of metal vacancies. Its associated chlorite is much more magnesian (Fe/Mg 0.6) than the chlorite in 15228 which has Fe/Mg ≈ 2.5 (Table 1, analysis 7). Alkali feldspar compositions are similar to those in 15228. The EPMA shows that the carbonate alteration zones contain calcite with ~1.5 wt.% MnO and low MgO and FeO (0.2 and 0.3 wt.%, respectively).

The nature of the feldspar alteration, and the presence of carbonate, patches of chlorite, and clusters of Ti-poor Fe-oxides reflects the regional sub-greenschist facies metamorphism (Oliver *et al.*, 1984). The mineralogy of the Eskdale intrusion is typical of granitic and granitic gneiss which are candidate GDF hosts. However, the altered granodiorite with its high chlorite, iron oxide and carbonate has mineralogical similarities to the late-stage, low-temperature, hydrothermal mineralized fractures that pervade ancient shield terranes, such as found in the Fennoscandanavian Shield which will host the Swedish GDF (Svensk Kärnbränslehantering, 2005; Stephens, 2010).

Borrowdale Volcanics Group (BV3)

In sample BV3 primary plagioclase phenocrysts are pseudomorphed by very fine-grained, low-temperature alteration products (clays and sericite) and 1 mm ×1 mm sized chlorite plus alteration product intergrowths are probably pseudomorphs after pyroxene. The fine-grained groundmass shows ophitic textures between irregular chlorite (or biotite grains) and euhedral altered feldspars.

An average analysis for the chlorite in BV3 is given in Table 1 (analysis 9); its Fe/Mg ratio is ~1.8 and, as mentioned above, Fe^{2+} is probably the main valency state. The feldspars include Na- and K-rich types as well as intermediate alkali feldspar solid solutions (Table 1, analysis 10) which probably points to the effects of alkali metasomatism during the pervasive alteration of primary pyroxene – calcic plagioclase intergrowths of the parental andesite. This BVG andesite sample demonstrates clearly the extreme hydrous alteration due to the sub-greenschist metamorphism to which the Lower Palaeozoic rocks have been subjected.

Jurassic mudstone (OM) and argillaceous limestone (JC)

The Oxford Clay (OM) is a very fine-grained, dark grey rock with small square or rounded pyrite grains (~5–50μm). X-ray diffraction shows the presence of abundant quartz and calcite, plus chlorite, sericite and illite; it is probable that the chlorite (Table 1 analysis 11) is associated with montmorillonite. The EPMA analyses confirm the presence of Na- and K-feldspar (Table 1, analyses 12 and 13) in the fine-grained matrix and that Ca-rich carbonates have 1.2 wt.% MgO and 0.22 wt.% FeO.

Sample JC has coarse calcite shell fragments set in a very fine-grained grey matrix of carbonate; small opaque grains (pyrite) are up to 0.25 mm in size and sometimes are composed of clusters of rounded sub-grains. The XRD traces suggest the presence of montmorillonite as an aluminous phase in the matrix. The EPMA analyses of carbonates confirm that both Ca-rich (0.7 wt.% MgO, 0.3 wt.% FeO) and Mg-rich varieties (CaO 32.5 wt.%, MgO 24.4 wt.%) are present.

St Bees sandstone (SBS)

The St Bees sandstone is composed mainly of sub-rounded clastic grains of quartz and some alkali-feldspar grains; minor Fe oxides are present. Clastic grains of muscovite, zircon and epidote are also present. The rock is stained red by the presence of fine-grained hematite and alkali feldspars and also shows much alteration to clay minerals; other alteration phases are fine-grained chlorite and sericite. X-ray maps for S and Ca suggest that anhydrite is a minor component. Analysis of the magnetite is given in Table 1 (analysis 14).

The St Bees sandstone will never be a GDF candidate but it may be present in the far field of a GDF; thus it illustrates the behaviour of an oxidized lithology with a large surface area of iron oxides, coating quartz grains and can also be considered as an 'end-member' Fe(III) standard.

Bulk rock analyses

The major-element analyses of the bulk rocks are given in Table 2. The high $H_2O(-)$ content in OM suggests the presence of smectite which might be present as montmorillonite/chlorite interlayers. The presence of S in the rock analyses is consistent with the presence of ~3 wt.% pyrite in OM and 1 wt.% in JC.

Sample OM is typical of many Jurassic and Carboniferous mudstones/clays in the UK; it is part of the same succession currently being assessed as a site for French geodisposal in the Paris Basin at Bure. Its clay-rich mineralogy, and significant carbonate content are also similar to the Lower Jurassic, Opalinus Clay from Mount Terri, Switzerland which has been used as a proxy for mudstone/clay rocks in the testing of potential GDF host rocks (Bossart and Wermeille, 1999; ANDRA, 2005). In contrast, the Lias sample (JC) is highly calcareous and more reduced, with a significant pyrite component of the Fe-budget. We will show later that the nature of fine-grained aluminosilicates is crucial in controlling the redox state of the rock/groundwater system.

Fe valence state and redox reactivity in rock samples

Electron Paramagnetic Resonance (EPR)

The EPR spectra were obtained to analyse key redox active species present with unpaired electrons, including Fe(III) and Mn(II). The EPR spectra for 15224 (Fig. 3*a*) and 15228 (Fig. 3*b*) are very similar, with peaks present at low field strengths ($g = 4.52$), indicating the presence of high-spin ($S = 5/2$) Fe(III) ions in sites of low symmetry, and the six-line hyperfine interaction at $g = 1.98$ from the nuclear spin of Mn55, indicating the presence of paramagnetic Mn(II) ions. Sample 15228 also shows a superoxide peak in the centre of the Mn (II) hyperfine splitting ($g = 2.00$) due to the valence electron hole in silicon and the O^{2-} radicals that are present in quartz (Plotze *et al.*, 2012). Sample BV3

TABLE 2. Results of XRF analyses of bulk rocks.

	Granite	Granite	Andesite	Sandstone	Mudstone	Argillaceous limestone
Wt.%	15228	15224	BV3	SBS	OM	JC
SiO_2	63.43	53.14	62.02	77.75	41.14	10.95
TiO_2	0.49	0.52	0.89	0.53	0.75	0.18
Al_2O_3	17.01	19.63	15.32	10.59	17.09	4.57
Fe_2O_3	1.63	0.56	1.05	2.32	4.01	1.29
FeO	2.58	3.25	6.25			
MnO	0.13	0.08	0.35	0.05	0.02	0.06
MgO	0.99	4.33	2.50	0.71	1.54	1.54
CaO	3.18	2.96	0.40	0.33	8.84	42.33
Na_2O	2.65	4.21	2.38	1.31	0.32	0.12
K_2O	5.28	5.58	5.64	4.75	2.73	0.85
P_2O_5	0.30	0.34	0.36	0.21	0.14	0.08
S	-	-	-	-	1.1	0.3
H_2O-	0	0.37	0	0.36	3.24	1.57
LOI	1.95*	4.80*	2.54*	0.72	17.09	35.84
Total	99.65	99.80	99.23	99.63	98.01	99.68
Traces (ppm)						
Rb	220	210	170	100	150	30
Sr	300	510	100	100	420	320
Ba	700	1080	1530	230	700	460
Zr	300	330	360	600	190	n.d.

*Corrected for weight gain due to oxidation of FeO during heating; n.d. – not determined; LOI – loss on ignition.

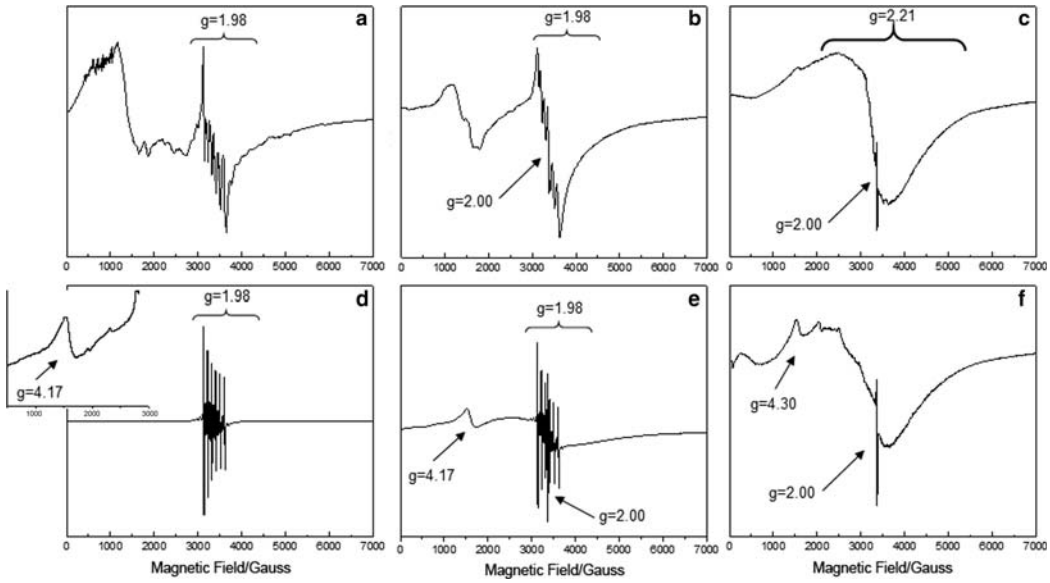

FIG. 3. EPR spectra: Eskdale granites 15224 (*a*) and 15228 (*b*), Borrowdale volcanic BV3 (*c*), Oxford clay OM (*d*), argillaceous limestone JC (*e*) and St. Bees sandstone SBS (*f*).

has the highest concentration of Fe (Table 2) and, as a result, the EPR spectrum (Fig. 3*c*) shows a broad feature at g = 2.21 due to ferromagnetic resonance (FMR) caused by Fe-Fe interactions. The super-oxide peak at g = 2.00 indicates the presence of quartz with defects. Samples JC and OM contain high concentrations of Mn resulting in EPR spectra (Figs 3*d*,*e*) with an intense signal at g = 1.98 due to Mn(II) hyperfine splitting. Both JC (Fig. 3*d* inset) and OM (Fig. 3*e*) show Fe(III) peaks at low field strengths (g = 4.17), and OM has a sharp superoxide peak at g = 2.00. As described in the previous section, SBS is composed mainly of hematite-covered quartz grains, thus, a large super-oxide peak at g = 2.0 is present in the EPR spectrum (Fig. 3*f*) and a low field strength Fe(III) signal at g = 4.3. The broad signal at mid-field suggests FMR as a result of Fe-Fe interactions. In summary, EPR shows: (1) the presence of Fe(III) ions in sites of low symmetry in all samples (with a detection limit of 0.01 μmol Fe(III)/g sample (Gustafsson *et al.*, 2014)); (2) the presence of Mn(II) in the granites, the clay and the mudstone; and (3) FMR in BV and SBS, which suggests Fe clustering in these samples.

X-ray Absorption Near Edge Spectroscopy (XANES)

The XANES spectra were collected at the Fe *K*-edge to obtain local structure and valence information as the Fe(III) absorption edge occurs at a higher energy than that for Fe(II) (Fig. 4). Wüstite (FeO), pyrite (FeS_2), biotite ($K(Mg, Fe)_3AlSi_3O_{10}(F, OH)_2$), magnetite ($Fe_3O_4$), hematite ($Fe_2O_3$) and Fe-rich montmorillonite were selected as Fe standards to obtain linear combination fits (LCFs) for these samples. The Fe(II)/Fe(III) ratios calculated from the LCFs (Table 3) show that BV3 and 15228 are highly reduced; 15224, JC and OM contain both Fe(II) and Fe(III) with increasing levels of oxidation, and SBS is almost fully oxidized.

Redox reactivity of rock samples before exposure to reducing groundwater

Redox reactivity of the Fe(II) in the ground-rock samples was determined by monitoring the reduction of the redox active dye, RBB. Reduction of the azo bonds in RBB will cause a decrease in the absorbance at the λ_{max} (597 nm), as described in Pearce *et al.* (2006). RBB is blue-black in colour and has two azo bonds in its structure, which can exist as either the azo tautomer (–N = N–) or the ketohydrazone tautomer (–HN–N =). The azo tautomer is preferentially reduced to produce a red molecule and a colourless amine, resulting in a purple colour, due to the presence of a mixture of the initial blue-black dye and the red reduction product. Complete reduction of the dye

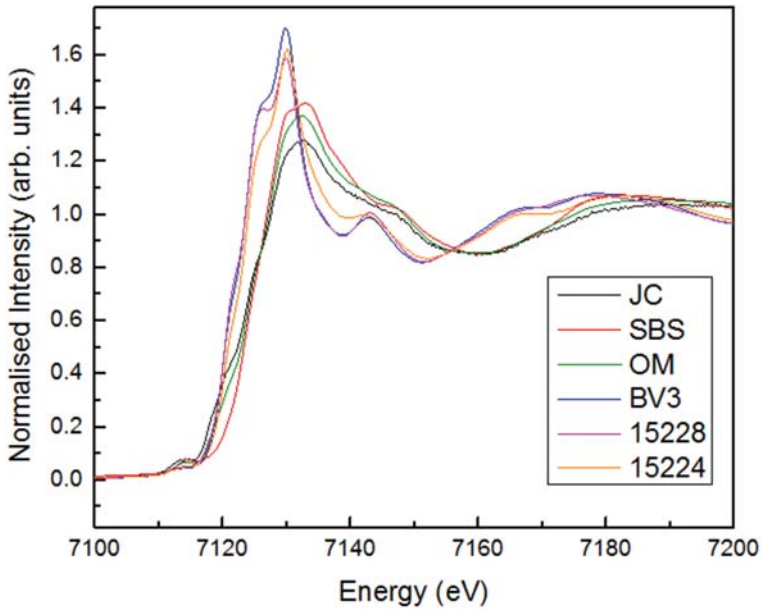

FIG. 4. Fe *K*-edge XANES spectra for Eskdale granites 15224 and 15228, Borrowdale volcanic, Oxford clay (OM), argillaceous limestone (JC) and St. Bees sandstone (SBS).

chromophore results in the production of colourless amines and requires eight electrons; therefore 8 moles of Fe(II) are required per mole of RBB (Pearce *et al.*, 2006). The change in absorbance at 597nm for the samples over a period of 60 days is shown in Fig 5. The two granites (15224 and 15228), BV3 and SBS did not exhibit any reducing potential towards RBB. Some reduction in the absorbance occurred with JC and OM, but this was due to sorption of the dye onto fine-grained clay-mineral surfaces and not azo bond reduction, as demonstrated by the lack of colour change (Fig. 5, inset). These results suggest that it is the Fe(II) mineralogy that controls the reactivity with the dye, not just the total Fe(II) concentration, and that the Fe(II) present within mineral grains in the original powdered-rock samples is unavailable for reaction with the dye. It is possible that the structural Fe(II) in these samples may have been oxidized at the surface due to air exposure, with the remaining Fe(II) content dispersed into mineral structures that do not allow electron density from the interior to be accessed at the surface. This has been shown for mixed valence magnetite, where Fe(II)-equivalents can migrate to the surface through the Fe–O–Fe– bridging network and react with oxidants in solution until a minimum Fe(II)/Fe(III) ratio is reached that maintains structural stability in the solid, at which point redox reactivity is lost, even though there is still Fe(II) present in the mineral phase (Liu *et al.*, 2012).

Redox reactivity of rock samples after exposure to reducing groundwater

Despite containing high concentrations of Fe(II), no RBB dye reduction was observed with the granites (15224 and 15228) or BV3. However, these samples had been stored dry, in air and it is likely that, in the long term, the conditions in the GDF will be water saturated and reducing. Thus, the rock samples were exposed to a reducing, Fe(II)-bearing model groundwater (typical Fe(II) concentrations in groundwater are 0.5–10 mg/l) to imitate the conditions over longer time periods in a GDF host-rock environment. The amount of Fe(II) uptake from solution by the rock samples is shown in Table 3. Samples 15224, JC and OM adsorbed all of the available Fe(II) from the groundwater. SBS adsorbed ~50% of the Fe(II). The rock samples containing the highest total Fe, the less altered granite (15228) and BV3, showed no evidence of Fe(II) adsorption, and instead an increase in the amount of Fe(II) in the groundwater was observed, as indicated by the negative values for Fe(II) uptake. This suggests that some of the relatively

TABLE 3. Fe valence state in untreated rock samples from LCF analysis of Fe *K*-edge XAS and their ability to uptake Fe(II) from a $FeCl_2$ (0.12mM) solution over a period of 10 days at room temperature

Mineral Phase Fe(II):Fe(III)	Wustite 100:0 (%)	Biotite 87:13 (%)	Pyrite 100:0 (%)	Magnetite 33:67 (%)	Hematite 0:100 (%)	Mont. 0:100 (%)	Fe(II)/Fe(III)	Fe(II) uptake (mM)
SBS	0.0	0.0	0.6	17.1	55.2	27.1	0.08	0.05
JC	0.0	8.7	36.3	2.6	22.3	30.1	0.70	0.12
OM	0.0	2.2	18.6	17.1	31.5	30.6	0.34	0.12
BV3	35.4	62.2	2.4	0.0	0.0	0.0	11.20	–0.07
15224	17.6	54.4	5.6	0.0	22.4	0.0	2.19	0.12
15228	33.3	55.9	10.8	0.0	0.0	0.0	7.84	–0.14

high concentrations of solid phase Fe(II) present in these samples was leached out into the groundwater over the 10 day period.

Redox reactivity of the rock samples after exposure to reducing groundwater was assessed using RBB dye as a probe molecule. For each rock, a control containing Fe(II)-bearing groundwater from the sorption experiments and RBB dye was used to determine whether dye reduction was caused by Fe(II) remaining in solution or by the structural and/or sorbed Fe(II) associated with the rock. In the controls, very little change in colour occurred showing that dissolved Fe(II) was not able to reduce the azo bonds over the timescale of the experiment. Reduction in absorbance at 597 nm over time is shown in Fig. 6. As expected, SBS displayed little dye reduction as it contains predominantly Fe(III)-bearing mineral phases. The less altered granite (15228) contained a significant amount of structural Fe(II) and would be expected to exhibit some reducing potential towards the dye. However, the Fe(II) is mainly in highly crystalline biotite grains, and these results suggest that although some of the Fe(II) within this phase is readily leachable (Table 3), the majority is not available for dye reduction. Sample BV3 was also expected to reduce the azo dye as the Fe in this sample is mainly Fe(II). However, the Fe(II) is present in chlorite and mica, which are also highly crystalline and, despite demonstrating a limited extent of dye reduction, the majority is not readily available for reaction. The more altered granite (15224), JC and OM showed the highest reducing potential. The colour change of the RBB dye from blue to purple to colourless (shown for JC in Fig. 6 inset) confirms that azo bond reduction, and not dye sorption, was responsible for the decrease in absorbance at 597 nm. JC and OM contain mainly Fe(III)-bearing mineral phases in the form of Fe-rich montmorillonite, thus these two samples were not expected to show any reducing potential. However, these samples absorbed the highest concentration of Fe(II) from groundwater in a form that was able to reduce the dye. The more altered granite (15224) contained predominantly Fe(II)-bearing minerals (phengite and chlorite) and it would be expected to behave similarly to 15228, i.e. limited dye reduction potential. However 15224 has a much more varied mineralogy than 15228 and is likely to contain clay minerals as alteration products of feldspars which resulted in significant adsorption of Fe(II) from the groundwater. These results show that the reducing potential was not correlated with the total

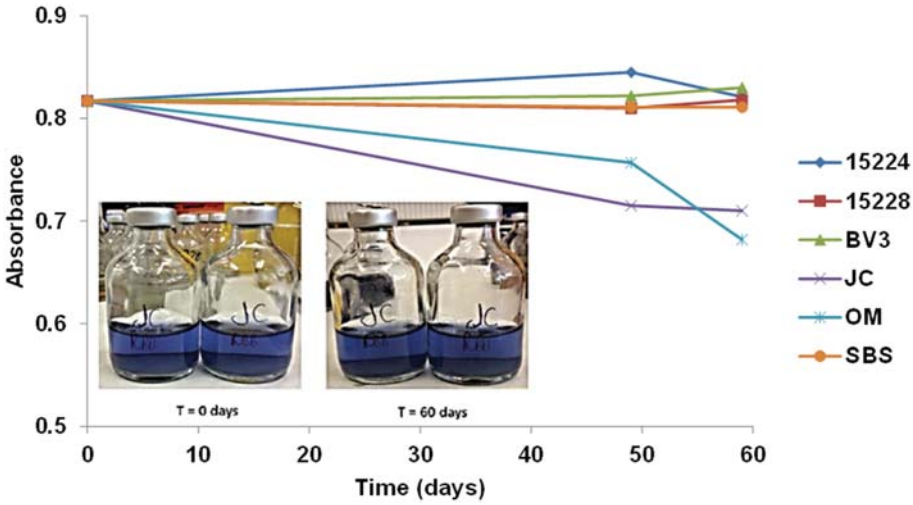

FIG. 5. Reduction in absorbance of RBB at 597 nm with time for untreated samples of Eskdale granites 15224 and 15228, Borrowdale volcanic (BV3), Oxford clay (OM), argillaceous limestone (JC) and St. Bees sandstone SBS. Inset showing RBB in the presence of JC before and after 60 days.

Fe(II) content of the rock, but with the ability of its mineral components to uptake Fe(II) from groundwater. Note that very little reduction of the azo dye was observed in the controls that contained only Fe(II) in solution, but without the rock samples (Fig. 6 inset). Previous work has suggested that homogeneous reduction by Fe(II) in solution is much slower than heterogeneous

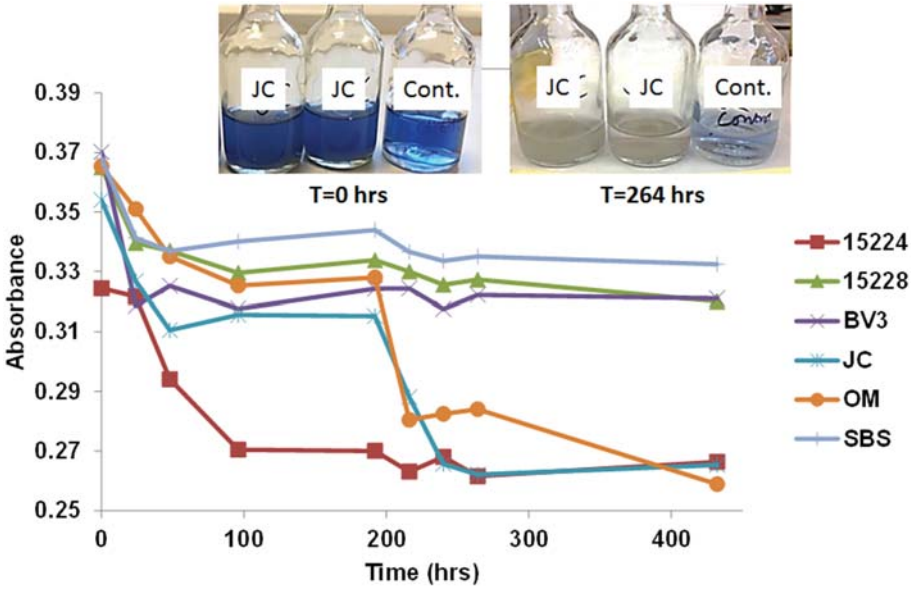

FIG. 6. Reduction in absorbance of RBB at 597 nm with time for samples of Eskdale granites 15224 and 15228, Borrowdale volcanic (BV3), Oxford clay (OM), argillaceous limestone (JC) and St. Bees sandstone (SBS) after exposure to Fe(II) solution. Inset showing RBB in the presence of JC and control before and after 264 hrs.

reduction catalysed by Fe(II) that is adsorbed onto mineral surfaces (Zachara *et al.*, 2007).

Conclusions

(1) It was expected that the two granitic rocks (15224 and 15228) and the Borrowdale volcanic (BV3) would exhibit the most reducing potential, as they were shown to have the highest concentration of structural Fe(II). No redox reactivity towards the reactive azo dye RBB was observed by any of the rock samples in their initial oxidation state, but the mudstone (OM) and argillaceous limestone (JC) were able to sorb the dye.

(2) The mudstone (OM), argillaceous limestone (JC) and the more altered granite rock sample (15224) were able to sorb all of the available Fe(II) from a reduced model groundwater; limited Fe(II) sorption was observed with the sandstone (SBS). The Borrowdale volcanic (BV3) and the less altered granite (15228) actually released Fe(II) into solution.

(3) The mudstone (OM), argillaceous limestone (JC) and the more altered granite (15224) reduced the azo dye to a much greater extent than the sandstone (SBS), less altered granite (15228) and Borrowdale volcanic (BV3). Thus it is not the Fe (II) in highly crystalline minerals within the rocks that determines the redox reactivity. Rather, it is the presence of fine-grained aluminosilicate alteration products, mainly clay minerals, that provide sorption sites for Fe(II) from reduced groundwaters which control the reducing potential of the rock.

(4) The mudstone (OM), argillaceous limestone (JC) and more altered granite (15224) could potentially be considered as more suitable host rocks for a GDF site as they demonstrate redox reactivity under reducing conditions, suggesting that they could reductively precipitate radionuclides such as uranium and technetium from their oxidized, soluble form, $U(VI)O_2^{2+}$ and $Tc(VII)O_4^-$, to their reduced, insoluble form, $U(IV)O_2$ and $Tc(IV)O_2$, thus restricting their mobility in the environment.

(5) A detailed study of the primary and alteration mineralogies and textural relations in potential host rocks for radioactive waste disposal provides important information on their suitability.

Acknowledgements

The authors thank John Charnock for supervising the EMPA analytical work, John Waters for XRD support, Paul Lythgoe and Alastair Bewsher for XRF analyses, Will Bower for providing XAS standards for LCF, the EPSRC UK National EPR Service at The University of Manchester and Diamond Light Source for access to beamline B18 (SP4941) that contributed to the results presented here.

References

ANDRA (2005) Synthesis: Evaluation of the feasibility of a geological repository in an argillaceous formation Meuse/Haute-Marne site. *ANDRA Report Series*. ANDRA, Châtenay-Malabry, France.

Barron, A.J.M., Lott, G.K. and Riding, J.B. (2012) Stratigraphical framework for the Middle Jurassic strata of Great Britain and the adjoining continental shelf. *Geology and Landscape Programme Research Report RR/11/06.* British Geological Survey, Keyworth, UK.

Bossart, P. and Wermeille, S. (1999) The Mont Terri rock laboratory. In: *Results of the hydrogeological, geochemical and geotechnical experiments performed in the Opalinus Clay (1996–1997)* (M. Thury and P. Bossart, editors). Geological report No. 23, Swiss Geological Survey.

Burley, S.D. (1984) Patterns of diagenesis in the Sherwood Sandstone (Triassic), UK. *Clay Minerals*, **19**, 403–440.

Deer, W.A., Howie, R.A. and Zussman, J. (1962) *Sheet Silicates.* Longman, London.

Department of Energy & Climate Change (2014) *Implementing Geological Disposal.* Department of Energy & Climate Change, London.

Droop, G.T.R. (1987) A general equation for estimating Fe3+ concentrations in ferromagnesian silicates and oxides from microprobe analyses, using stoichiometric criteria, *Mineralogical Magazine*, **51**, 431–435

Fleet, M.E. (2003) *Rock-Forming Minerals, Vol. 3A: Micas.* The Geological Society, London, pp. 765.

Gustafsson, H., Hallbeck, M., Norell, M., Lindgren, M., Engström, M., Rosén, A. and Zachrisson, H. (2014) Fe(III) distribution varies substantially within and between atherosclerotic plaques. *Magnetic Resonance in Medicine*, **71**, 885–892.

Hesselbo, S.P. (2008) Sequence stratigraphy and inferred relative sea-level change from the onshore British Jurassic. *Proceedings. of the Geological Association*, **119**, 19–34

Holliday, D.W., Jones, N.S. and McMillan, A.A. (2005) Lithostratigraphical subdivision of the Sherwood Sandstone Group (Triassic) of the northeastern part of the Carlisle Basin, Cumbria, and adjacent parts of Dumfries and Galloway, UK. *Geology & Landscape Northern Britain Programme Internal Report IR/05/148.* British Geological Survey, Keyworth, UK.

Kiriakoulakis, K., Marshall, J.D. and Wolff, G.A. (2000) Biomarkers in a Lower Jurassic concretion from Dorset (UK). *Journal of the Geological Society*, **157**, 207–220.

Liu, J., Pearce, C.I., Qafoku, O., Arenholz, A., Heald, S. M. and Rosso, K.M. (2012) Tc(VII) reduction kinetics by titanomagnetite ($Fe_{3-x}Ti_xO_4$) nanoparticles. *Geochimica et Cosmochimica Acta*, **92**, 67–81.

MacQuaker, J.H.S. (1994) A lithofacies study of the Peterborough Member, Oxford Clay mudstone succession Formation (Jurassic), UK: an example of sediment bypass in a mudstone sequence. *Journal of the Geological Society*, **151**, 161–172.

Millward, D. (2004) A stratigraphical framework for the upper Ordovician and Lower Devonian volcanic and intrusive rocks in the English Lake District and adjacent areas. *Integrated Geoscience Surveys (North) Programme Research Report RR/01/07*. British Geological Survey, Keyworth, UK.

Milodowski, A.E., Gillespie, M.R., Naden, J., Fortey, N.J., Shepherd, T.J., Pearce, J.M. and Metcalfe, R. (1998) The petrology and paragenesis of fracture mineralization in the Sellafield area, West Cumbria. *Proceedings of the Yorkshire Geological Society*, **52**, 215–241.

Nuclear Decommissioning Authority [NDA] (2010) *Geological Disposal: Generic Environmental Safety Case main report.* NDA report no. NDA/RWMD/021. Didcot, UK.

Oliver, G.J.H., Smellie, J.L., Thomas, L.J., Casey, D.M., Kemp, A.E.S., Evans, L.J., Baldwin, J.R. and Hepworth, B.C. (1984) Early Palaeozoic metamorphic history of the Midland Valley, the Southern Uplands-Longford-Down massif and the Lake District, British Isles. *Transactions of the Royal Society of Edinburgh: Earth Science*, **75**, 259–273.

Pearce, C.I., Christie, R., Boothman, C., von Canstein, H., Guthrie, J.T. and Lloyd, J.R. (2006) Reactive azo dye reduction in Shewanella strain J18 143. *Biotechnology and Bioengineering*, **95**, 692–703.

Peters, T.J. and Hofmann, B. (1984) Hydrothermal clay mineral formation in a biotite granite in northern Switzerland. *Clay Minerals*, **19**, 579–590.

Plötze, M., Wolf, D. and Krbetschek, M.R. (2012) Gamma-irradiation dependency of EPR and TL-spectra of quartz. Pp. 177–190 in: *Quartz: Deposits, Mineralogy and Analytics* (J. Götze, and R. Möckel, editors). Springer, Berlin.

Psyrillos, A., Howe, J.H., Manning, D.A.C. and Burley, S. D. (1999) Geological controls on kaolin particle shape and consequences for mineral processing. *Clay Minerals*, **34**, 193–208.

Simpson, B. (1934) The petrology of the Eskdale (Cumberland) Granite. *Proceedings of the Geological Association*, **XLV**, 17–34.

Svensk Kärnbränslehantering [SKB] (2005) *Extended consultations according to the environmental code.* EnaInfo/Edita Norstedts Tryckeri, Swedish Nuclear Fuel and Waste Management Co, Stockholm.

Stephens, M.B. (2010) *Forsmark site investigation: Bedrock geology – overview and excursion guide.* SKB R-10-04. Svensk Kärnbränslehantering, Swedish Nuclear Fuel and Waste Management Co, Stockholm, pp. 52.

Stookey, L.L. (1970) Ferrozine – A new spectrophotometric reagent for iron. *Analytical Chemistry*, **42**, 779–781.

Young, B., Fortey, N.J. and Nancarrow, P.H.A. (1986) An occurrence of tungsten mineralisation in the Eskdale Intrusion, West Cumbria. *Proceedings of the Yorkshire Geological Society*, **46**, 15–21.

Zachara, J.M., Heald, S.M., Jeon, B.-H., Kukkadapu, R. K., Liu, C., McKinley, J.P., Dohnalkova, A.C. and Moore, D.A. (2007) Reduction of pertechnetate [Tc (VII)] by aqueous Fe(II) and the nature of solid phase redox products. *Geochimica et Cosmochimica Acta*, **71**, 2137–2157.